ISSN: 0067-2904

Synthesis of $CdFe_2O_4$-SnO_2 Nano Spinel Ferrite and Investigation of the Structural and H_2S Gas Sensing Properties

Mariam O. Abd Alkareem* ,Tagreed M. Al-Saadi
College of Education for Pure Science, Ibn Al Haitham, University of Baghdad, Baghdad, Iraq

Received: 17/11/2024 Accepted: 1/7/2025 Published: 30/6/2026

ABSTRACT

In this paper, nanoferrite ($CdFe_2O_4$-SnO_2) was prepared by the auto combustion method (sol-gel), with weight ratios of (x = 0.0, 0.05, 0.10, 0.15, 0.20, 0.25) for SnO_2. The properties of the nanoferrite were characterized by XRD, FE-SEM, and EDX techniques. The results showed that the produced compound had a cubic spinel ferrite phase; the crystallite size was determined using the Scherrer and Williamson-Hall equation. The FE-SEM image demonstrated that the compound is porous, with nanoscale particles that have a ball-like appearance. The EDX test verified the existence of Fe, O, Cd, and Sn atoms. Gas sensing showed the compound's high sensitivity to H_2S.

Keywords: NanoFerrite, Cd-ferrite, doped SnO_2, Structural properties, H_2S gas, Sensitivity

تحضيرفيريت السبينيل النانوي $CdFe_2O_4$-SnO_2 ودراسة خصائصه التركيبية واستشعار غازH_2S

مريم اسامة[1]، تغريد مسلم[2]*

كلية التربية للعلوم الصرفة -ابن الهيثم ، جامعة بغداد، بغداد، العرا ق

تم في هذا البحث تحضير نانو فيريت ($CdFe_2O_4$–SnO_2) بطريقة الاحتراق الذاتي (سول–جل) مع نسبة وزن (0، 0.05، 0.10، 0.15، 0.20، 0.25) من SnO_2. تم تحديد خصائص النانو فيريت باستخدام تقنيات XRD و FE–SEM وEDX. أظهرت النتائج أن المركب الناتج له طور فيريت سبينيل مكعب؛ تم تحديد حجم البلورة باستخدام معادلة شيرر ووليامسون–هول. أظهرت صورة FE–SEM أن المركب مسامي، مع جزيئات نانوية ذات مظهر كروي. أكد اختبار EDX وجود ذرات Fe و O و Cd وSn، وأظهر استشعار الغاز حساسية عالية للمركب لغاز H_2S .

1. Introduction

Hydrogen sulfide (H_2S) is an important industrial pollution gas that can seriously damage a person's health [1]. It also contributes to the formation of acid rain. Therefore, there is a critical need to develop efficient H_2S sensors capable of continuously monitoring the environment [2]; they respond well to H_2S gas because of their increased stability and inexpensive cost, which often exhibit a greater reaction to H_2S at high temperatures [3], although, H_2S is a flammable and explosive gas that can potentially identify safety problems at high operating temperatures [4].

*Email: taghreed.m.m@ihcoedu.uobaghdad.edu.iq

The chemical formula for spinel ferrite is MFe_2O_4, where M-denotes divalent metal ions, such as Cd, Mn, Co, Ni, etc. It has two sub lattices, tetrahedral A and octahedral B [5]. The chemical composition and structure of spinel ferrites, when transition or post-transition cations are present and occupy two distinct cation positions, are the most intriguing aspects of these materials for gas detection [6]. Since the spinel ferrites are inexpensive, have simple electronic structures, and are stable in thermal and chemical atmospheres, they have demonstrated high sensitivity for various gases [7]. Several chemical methods, including sol-gel [8], microemulsion [9], and chemical co-precipitation [10], have been employed for the manufacture of ferrite nanoparticles.

Sol-gel is a commonly utilized technique to create ferrite nanoparticles. The fuel, pH, stirring duration, speed, metal nitrate to fuel ratio, and other factors can all have a significant impact on the size and characteristics of spinel ferrite nanoparticles [11]. According to the Fd3m space group, cadmium ferrite has a normal spinel structure [12]. In this structure, site A is occupied by $8M^{2+}$(divalent metallic) ions, while site B is fully filled with 16 Fe^{3+} ions. There is no inversion parameter for a normal spinel. When trivalent cations are filled at B sites, this type of dissemination or arrangement is referred to as normal spinel [13]; the spinel-type semiconductor $MgFe_2O_4$ and $CdFe_2O_4$ have demonstrated sensitivity and selectivity to Liquefied Petroleum Gas (LPG) and C_2H_2, as reported in [14].
Previous studies have shown that tin ions have a positive effect on increasing the sensitivity of magnesium ferrite to the acetone gas [15-16]. Tin added to $MgFe_2O_4$ promotes the oxidation of the reducing gas and the creation of oxygen vacancies, which changes the electrical conductivity. The change in electrical conductivity is caused by the gas molecules' chemical interaction with the oxygen absorbed on the surface of the metal oxide, which is the sensing mechanism for reducing gases [17]. Manikandan et al. generated nanocrystalline tin replacing copper ferrite ($Sn_{0.2}Cu_{0.8}Fe_2O_4$) by employing a co-precipitation technique. With 90% reproducibility and high stability, the developed $Sn_{0.2}Cu_{0.8}Fe_2O_4$gas sensor responded to 2 vol% LPG with 78.78%. The incorporation of tin in copper ferrite developed $Sn_{0.2}Cu_{0.8}Fe_2O_4$ gas sensor showed promising effects toward LPG at room temperature, indicating its potential for LPG detection in real applications [18].

This study employs a simple sol-gel method to synthesize $CdFe_2O_4$-SnO_2 nano ferrite. This composition was specifically selected due to its enhanced sensitivity in gas-sensing applications. Significant improvements in response and recovery times were found when it was used as a hydrogen sulfide (H_2S) gas sensor. The findings and their significance for the advancement of gas sensors in the future are highlighted in the presentation and discussion of the findings.

2. Experimental

2.1. Preparation

The sol-gel method was used to create the $CdFe_2O_4$-SnO_2 with different weight ratios of SnO_2 (x = 0.00, 0.05, 0.10, 0.15, 0.20, 0.25). The following raw ingredients were utilized in the synthesis process: cadmium nitrate (Cd $(NO_3)_2.4H_2O$) of 308.48g/mol molecular weight, tin chloride (stannic chloride pentahydrate) ($SnCl_4.5H_2O$) of 350.5984g/mol molecular weight, ferric nitrate (Fe $(NO_3)_3.9H_2O$) of 404g/mol molecular weight, and citric acid ($C_6H_8O_7$). Table 1 illustrates the quantities of the basic ingredients needed to make nano-ferrite; the following formula was used to calculate the mass of the reactants [19]:

$$\text{Wt. (g)} = M_w\text{(g/mol)} \times \text{M(mol/L)} \times \text{V(L)} \quad (1)$$

Where Wt. denotes the raw material's mass, M_w is its molecular weight, M is the number of moles needed to dissolve the material in one liter of solvent and V is the solvent's volume.

A heat-resistant glass beaker containing 1000 mL of deionized water was filled with mineral nitrate. Citric acid was added to 40 ml of deionized water in a different glass beaker. Then, without heating, the nitrate solution and the acid solution were combined using a magnetic stirrer; ammonia was added in drops to the mixture to form a homogenous solution of pH ~7. The metal nitrates and citrate molecules undergo a combustion event that results in a polymer network with colloidal dimensions known as a sol [20]. The temperature reached 80°C when the magnetic mixing heater was turned on. During the mixing process, the mixture was heated until a gel formed; with continued heating, the gel ignited. It was then left to cool and heated in the oven resulting in a powder. A manual pressing machine was used to press the powder at 1.5 ton/cm^2 pressure. The resultant pellets, which had a 1 cm diameter and 2.5 mm thickness, were subsequently sintered at 900 °C for two hours.

Table 1: The molar numbers (n) and mass (w) of the components utilized to prepare the nano-ferrite samples.

Composition	Ferric nitrate		Cadmium nitrate		Tin chloride		Citric acid	
	n	m(g)	n	m(g)	Content x%	m(g)	n	m(g)
$CdFe_2O_4$	2	32.32	1	12.3392	0	0	3	23.0556
$CdFe_2O_4$-$SnO_{2\ (0.05)}$	2	32.32	1	12.3392	5	0.61696	3	23.0556
$CdFe_2O_4$-$SnO_{2\ (0.10)}$	2	32.32	1	12.3392	10	1.23392	3	23.0556
$CdFe_2O_4$-$SnO_{2\ (0.15)}$	2	32.32	1	12.3392	15	1.85088	3	23.0556
$CdFe_2O_4$-$SnO_{2\ (0.20)}$	2	32.32	1	12.3392	20	2.46784	3	23.0556
$CdFe_2O_4$-$SnO_{2\ (0.25)}$	2	32.32	1	12.3392	25	3.0848	3	23.0556

2.2. Measurement

the structural and sensing properties of the resulting composites were studied using: XRD diffractometer (Philips PW1730) with the following features: target material (Cu), wavelength (Kα): λ=1.5406 Å, range (2θ): 20° to 80°, current: 40 mA, and voltage: 40 kV; Field Emission Scanning Electron Microscope (FE-SEM) (MIRA3 LMU) to determine accurate and comprehensive study of the surface topography, content, and size of the nanoparticles; Energy-Dispersive X-ray (EDX) analyzer to determine the percentage of each component that makes up the final nanocomposites.

The gas sensing system shown in Figure 1 was used to measure the sensitivity to changes in sample resistance when exposed to H_2S gas, with measurements conducted at temperatures 200, 250, and 300°C. The gas sensing system was used to determine the optimum operating temperature.

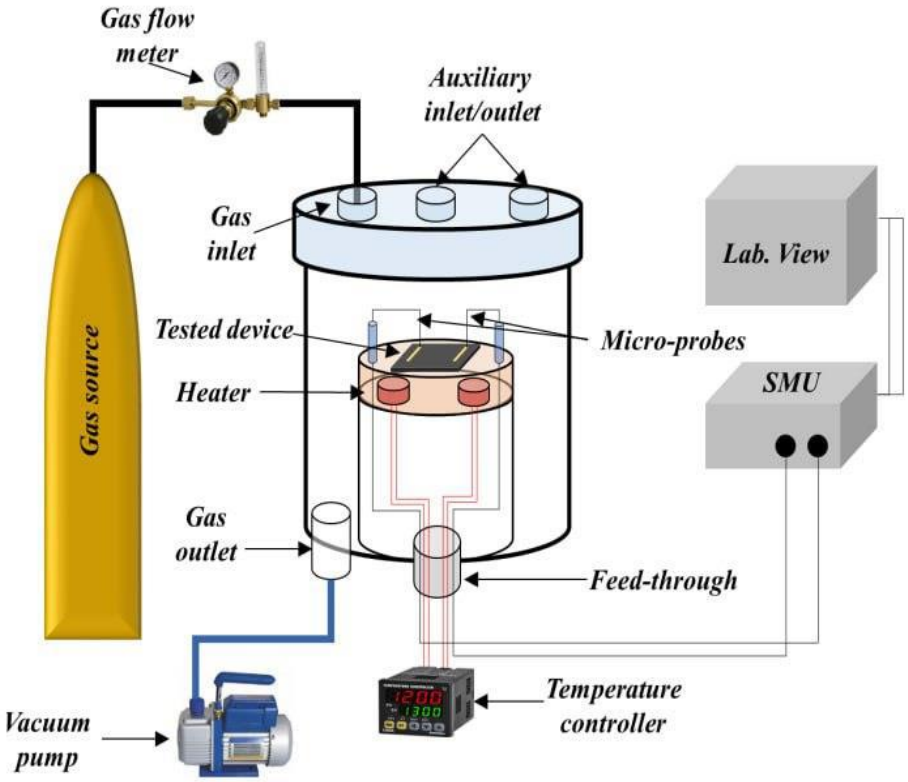

Figure 1: Gas sensing system [20]

3. Results and discussion

3.1 X-ray diffraction analysis

The X-ray diffraction pattern of the cubic spinel structure exhibited a high degree of crystallinity across the whole structure, as shown in Figure 2. The diffraction peak degree in all prepared samples and the main reflection planes (220), (311), (222), (400), (422), (511), and (440) that correspond to the cubic spinel structure were observed. The results agree with the international standard file of $CdFe_2O_4$ diffraction data card JCPDS No. (22-1063).

In addition, the X-ray diffraction patterns show some secondary peaks. The most prominent of these peaks is at position 24.1°, which is attributed to the α-Fe_2O_3 (hematite) phase (JCPDS No. (84-0311)). The primary reason is the oxidation of Fe_3O_4. Fe_3O_4 (magnetite) contains both Fe^{2+} and Fe^{3+} ions. If exposed to oxygen during synthesis, Fe^{2+} oxidizes to Fe^{3+}, forming α-Fe_2O_3. This is particularly common in nanoparticle synthesis, where high surface area makes Fe_3O_4 more susceptible to oxidation. Several reasons explain the decrease or disappearance of some peaks, including the formation of secondary phases as α-Fe_2O_3 or SnO, or a change in the crystal size and stress distribution in the crystal lattice, and others [21].

Lattice parameters were calculated using the "Match! 3" software, and the mean crystallite size (D_{Sh}) was calculated using Scherrer equation [22]:

$$D_{Sh} = 0.9\lambda / \beta \cos\theta \quad (2)$$

Where λ is X-ray wavelength (1.54 Å), β is full width at half maximum, and θ is Bragg angle. The X-ray density (ρ) can be calculated using the following equation [23,24]:

$$\rho = 8Mw / N_A . a^3 \quad (3)$$

Where (M_W) is the molecular weight, (N_A) is the Avogadro number, and (a) is the constant lattice.

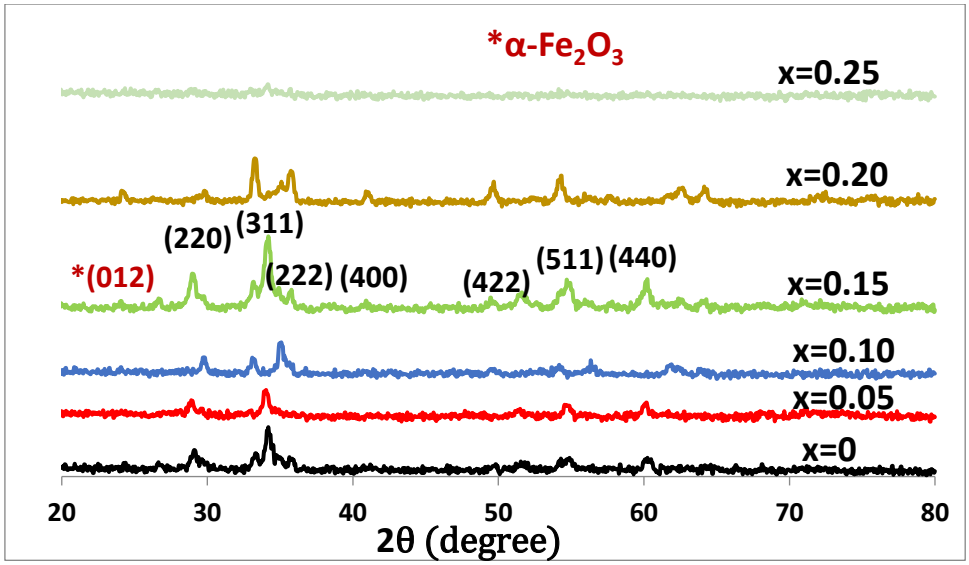

Figure 2: X-Ray diffraction patterns of $CdFe_2O_4$-SnO_2 nano-ferrite for different weight ratios of SnO_2.

Table 2 indicates that the addition of tin to cadmium ferrite did not increase the lattice constant, although the ionic radius of cadmium ion (92 pm) and tin ion (122 pm) are much greater than the ionic radius of iron (63pm) due to the transfer of iron ions between octahedral and tetrahedral sites, this agrees with Ahmad et al. [25], in cadmium ferrites with natural spinel structure, divalent cadmium ions occupy the tetrahedral sites while trivalent iron ions occupy octahedral sites. However, reports of mixed spinel structures are often seen in nanocrystalline cadmium ferrites, with cadmium cations found in both tetrahedral and octahedral. The specific cation distribution influences the physical parameters of this semiconductor ceramic [26]. The distance between magnetic ions at the tetrahedral site (L_A) and that at the octahedral site (L_B) is determined by the hopping length [27]:

$$L_A = 0.25a\sqrt{3} \quad (4)$$

$$L_B = 0.25a\sqrt{2} \quad (5)$$

Tin ions can be found with a hopping length of (3.970-3.670 Å) in octahedral sites and a hopping length of (3.071-3.095 Å) in tetrahedral sites. The electron hopping between ion pairs in the octahedral and tetrahedral sites of tin ions is due to the exchange coupling between ions in these sites.

The crystallite size was determined using Scherrer relation (Eq. 2). Table 2 shows that the introduction of tin led to structural changes in the porosity and grain size. The granularity of tin-containing grains was observed to be approximately (23.07-36.24nm) [28].

The grain size was computed using the Williamson-Hall equation [29, 30]

$$\beta_{hkl} = (K\,\lambda/D) + 4\varepsilon \sin\theta \quad (6)$$

Where K is constant, λ is the Cu Kα radiation wavelength, D is the average grain size, and ε is the microstrain. The equation was plotted with sinθ on the x-axis and β cosθ on the y-axis, as illustrated in Figure 3, for all samples the average crystallite size and microstrain were obtained from the slope and y-axis intercept of the fitted line corresponding to the intercept Kλ/D and the 4ε, respectively. Table 2 shows that the microstrain values are negative for all samples except the sample $CdFe_2O_4$; this is because the introduction of tin led to the shrinkage of the lattice with a decrease in the lattice constant. It is observed that the lattice constant did not rise linearly as predicted by Vegard law when the weight ratio of tin increased because of defects in magnetic nano oxide structure; oxygen vacancies, lattice distortion, local disturbances, and rotational deviation can alter the bond length by influencing the ions equilibrium locations inside the spinel structure [19, 31].

Table 2: Lattice constants, density and crystallite size of $CdFe_2O_4$-SnO_2 nano-ferrite

X (SnO_2 Content)	Lattice constant (Å)	Density (g/cm^3)	D Scherrer (nm)	D Williamson-Hall (nm)	Microstrain 10^{-3}	Hopping Length L_A (Å)	Hopping length L_B (Å)
0	8.7153	5.783	26.48	17	8.865	3.773	3.081
0.05	8.6883	5.836	25.51	6.3	-6.488	3.762	3.071
0.10	8.4770	5.909	36.24	8.7	-5.475	3.670	2.997
0.15	8.7003	6.249	28.33	10.8	-3.35	3.767	3.076
0.20	8.7069	6.210	23.07	12.70	-2.535	3.770	3.078
0.25	8.7541	5.782	28.94	4.3	-10.543	3.790	3.095

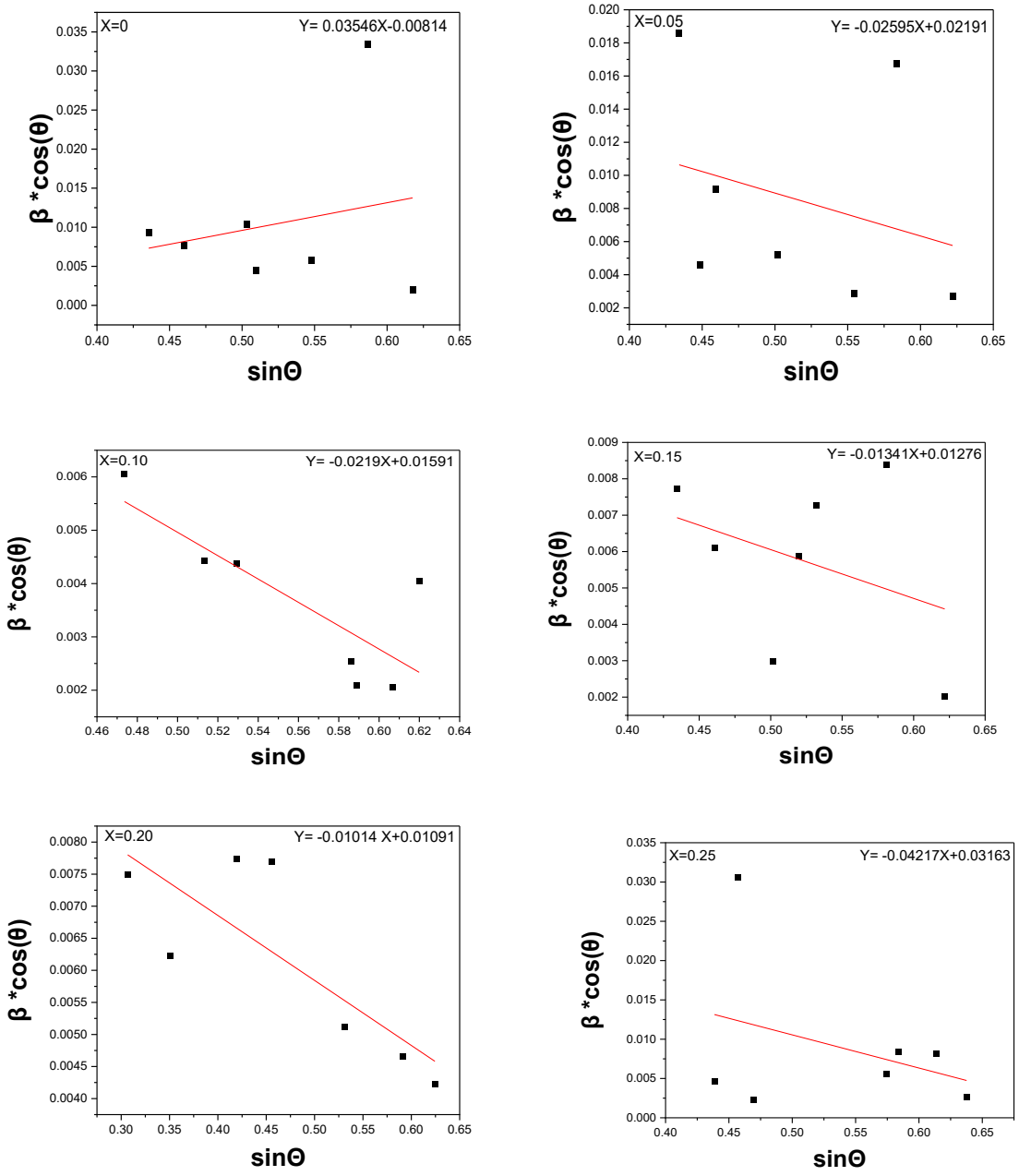

Figure 3: Williamson-Hall analysis of $CdFe_2O_4$-SnO_2 nanoparticles

Using the Scherrer and Williamson-Hall methods, a comprehensive assessment of crystal size can be obtained, which helps ensuring the accuracy of the results and provides a deeper analysis of the structural properties. The Scherrer method relies on measuring the peak width in the spectrum and gives a direct estimate of the crystal size through the peak width. The Williamson-Hall method considers the effect of internal and microscopic distortions, which makes it more accurate and helps in understanding the relationships between crystal size and structural defects.

3.2. Morphological analyses

Images of $CdFe_2O_4$-SnO_2 (x = 0.0, 0.15, 0.25) nanoparticles' surface morphology are displayed in Figure 4. These images proved that the prepared samples were mostly spherical on the nanoscale. The structures described in this work have tiny grain sizes and porosity, which increases the sample's specific surface area to be suitable for gas sensing applications [32, 33]. When specific clusters or accumulations are present, the porous quality of the substance's surface, required for gas adsorption, is represented by the voids that exist between the region's agglomerations or conglomerates [34]. Figure 4 displays the synthesized samples' grain size distribution, which was calculated statistically using the lognormal distribution based on the scanning electron microscope (FE-SEM) image. It demonstrated that the sample's particle size varied between 38.83 to 74.17 nm. In contrast to the crystal sizes found in the XRD pattern, there are some agglomerations in different places that resulted in the higher particle sizes in nanoferrites caused by Van der Waals forces and magnetic dipole interactions, which are rather strong interactions between magnetic particles [35].

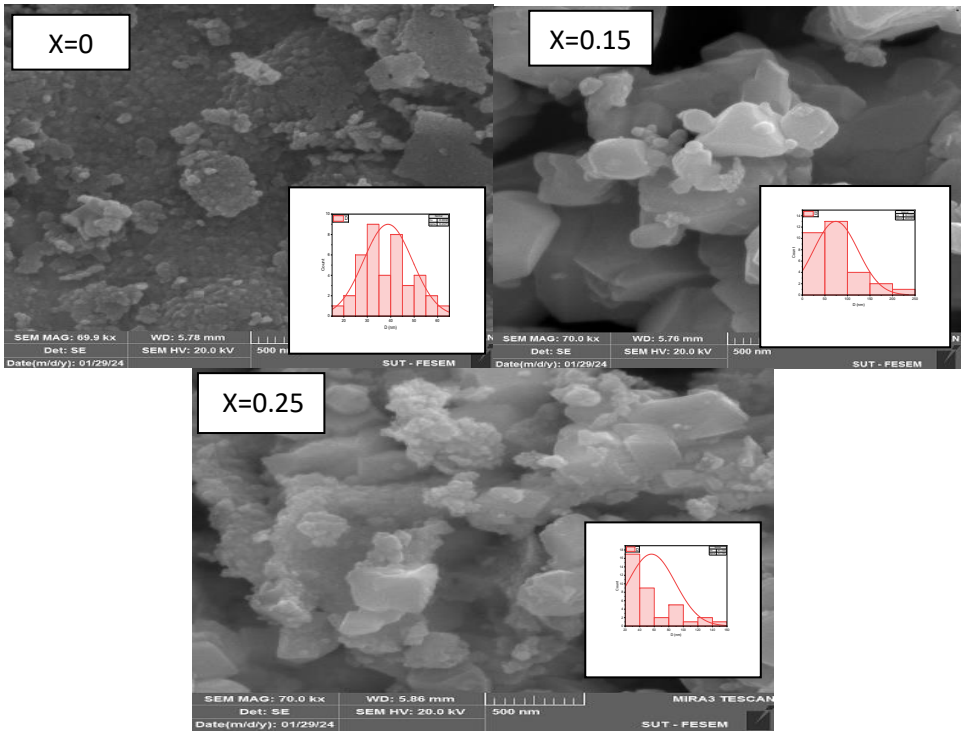

Figure 4: FE-SEM of $CdFe_2O_4$ - SnO_2 ferrite nanoparticles samples.

3.3. Elemental analysis

The EDX analysis of $CdFe_2O_4$-SnO_2 nanoferrite is displayed in Figure 5 and Table 3. EDX examination of this spectrum verified the existence of Fe, Cd, Sn, and O components; by measuring the energy difference between the outer shells and the atomic structure of the

element [36], no other components or impurities were found. This validates the generated samples' purity, which is supported by the XRD data. This is because the spontaneous combustion method is very effective [37].

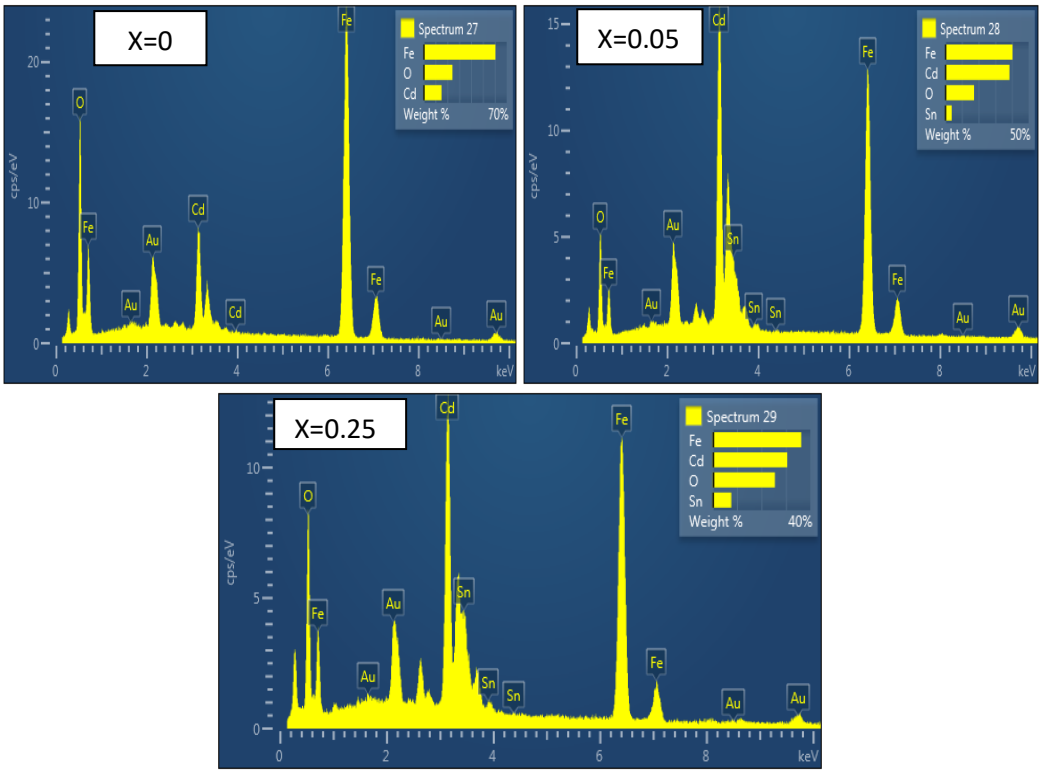

Figure 5: EDX of the nanoferrite samples $CdFe_2O_4$-SnO_2

Table 3: The weight and atomic ratios of the elements present in the prepared samples

Sample	Element	Energy (keV)	Line Type	Wt%	Atomic%
$CdFe_2O_4$	O	0.525	Kα	24.30	55.48
	Fe	6.405	Kα	60.54	39.59
	Cd	3.133	Lα	15.16	4.93
	Total			100.00	100.00
Sample	Element		Line Type	Wt%	Atomic%
$CdFe_2O_4$-$SnO_{2(0.05)}$	O	0.525	Kα	17.28	49.59
	Fe	6.405	Kα	40.33	33.17
	Cd	3.133	Lα	38.51	15.74
	Sn	3.444	Lα	3.88	1.50
	Total			100.00	100.00
Sample	Element		Line Type	Wt%	Atomic%
$CdFe_2O_4$-$SnO_{2(0.25)}$	O	0.525	Kα	25.52	61.80
	Fe	6.405	Kα	36.27	25.16
	Cd	3.133	Lα	30.55	10.53
	Sn	3.444	Lα	7.66	2.50
	Total			100.00	100.00

3.4. Sensing Properties of $CdFe_2O_4$-SnO_2 nano-ferrite

The sensing of hydrogen sulfide gas (H2S) works by its reaction with adsorbed oxygen, which releases electrons back into the sensing material. This reaction occurs when the sensor (ferrite compound) is exposed to the reducing gas. The trivalent cation M^{+3} undergoes a reduction process that turns it into the bivalent cation M^{+2}, as shown by the following equation [38].

$$M^{+3} + e^- \rightarrow M^{+2} \quad (7)$$

This will result in a decrease in the voltage barrier area (electron depletion area), a decrease in the resistance to the flow of electrons, and thus greater freedom for electrons to move and an increase in the conductivity of the sensor. Figure 6 shows the electron depletion zone, where controlling this region can lead to significant improvements in conductivity.

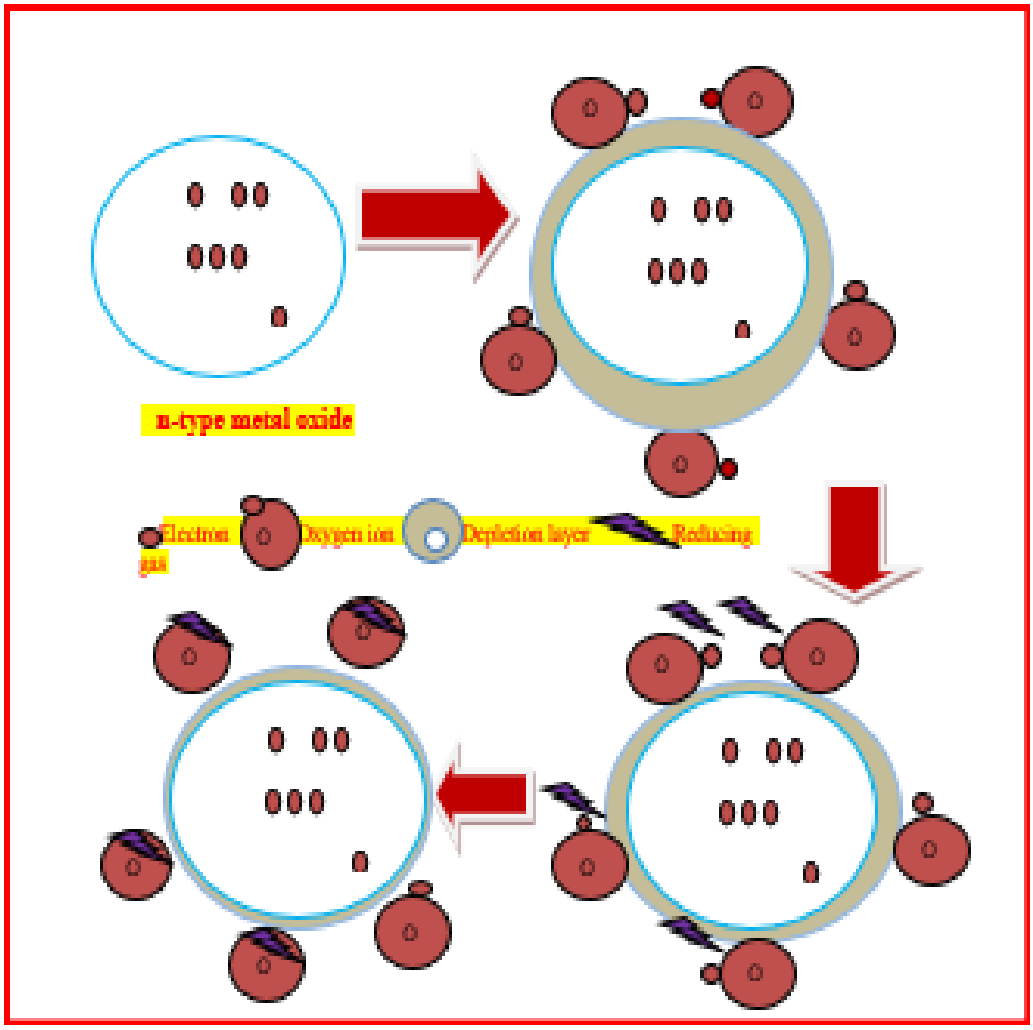

Figure 6: Schematic diagram of the mechanism sensing n-type metal oxide for reducing gas

The definition of the sensor response (S) is the ratio of the resistance change (R_g-R_a) with the air sensor resistance (R_a) following exposure to the goal analytics.

$$S = (|R_a - R_g|) / R_g \times 100\% \quad (8)$$

Where R_a and R_g denote the sensor's resistances in air and analyte gas, respectively. To evaluate the response and recovery time, the sensor's time was set to achieve 90% of the total change in resistance from its initial resistance [39, 40] .The sensitivity of $CdFe_2O_4$-SnO_2 to reduce the (H_2S) gas was investigated at various operating temperatures (200-250-300°C), as shown in Figure 7 and Table 4.

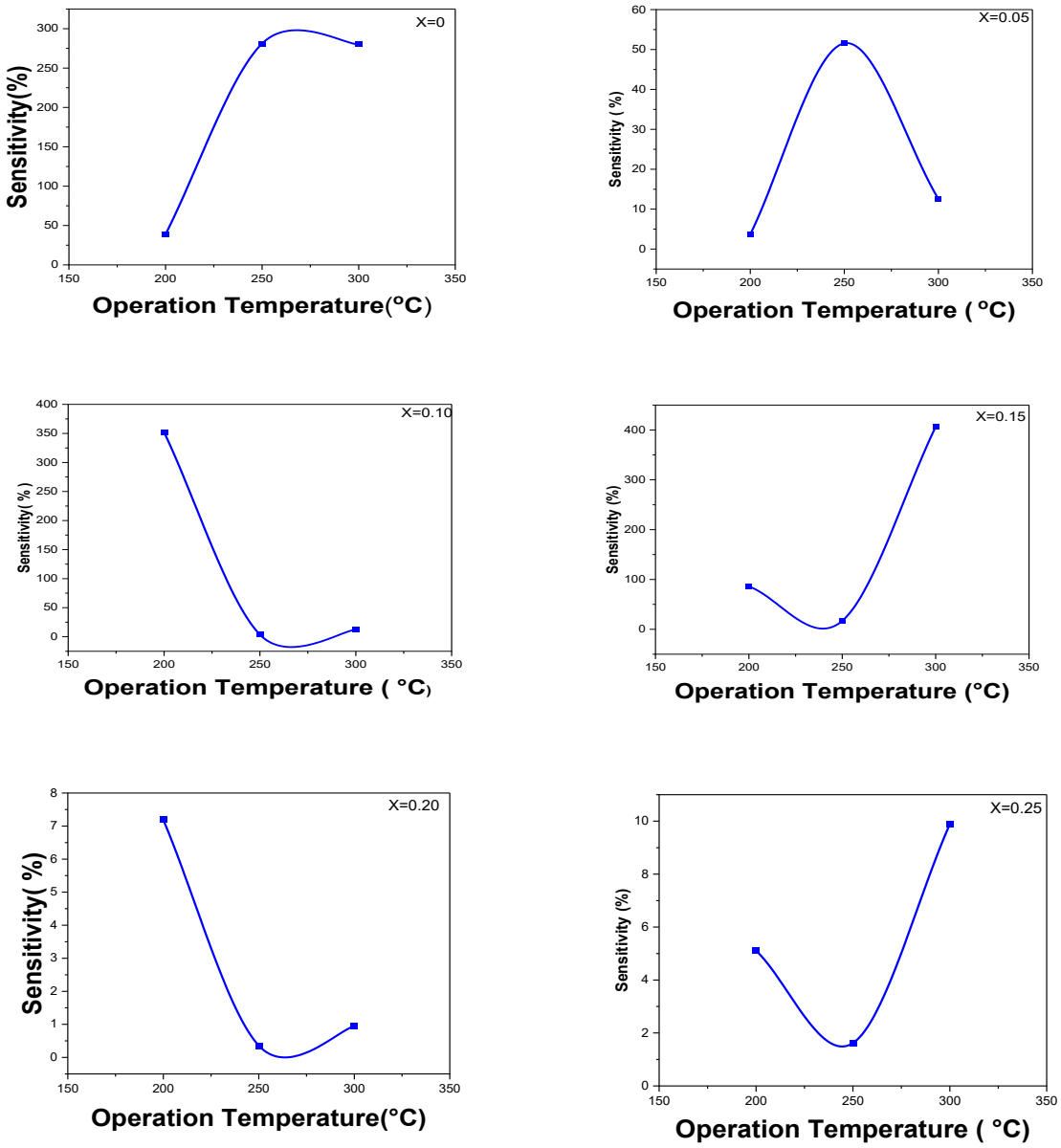

Figure 7: The sensitivity versus operating temperature of $CdFe_2O_4$-SnO_2 sample.

Table 4: The maximum sensitivity values for the $CdFe_2O_4$ -SnO_2 samples and it is noteworthy that the maximum sensitivity value was at 300°C.

x Content	Operating Temperature	Highest sensitivity value (%)
0	250°C-300°C	281
0.05	250°C	51.544
0.10	200°C	352.380
0.15	300°C	406.429
0.20	200°C	7.193
0.25	300°C	9.88

The characteristics of the gas sensors showed that the operating temperature and SnO_2 concentration affect the sensitivity to H_2S gas. Tin is a well-known additive that is highly effective at activating and promoting the surface reaction process of gas-sensing materials,

thus improving their performance [41]. This is attributed to the fact that tin contains a d10 electronic configuration and double valence state; the presence of these electrons in the d level can contribute to improving electrical conductivity, which enhances tin's ability to interact with electric fields, which is useful for improving sensing [20]. As for the samples (x = 0.05, 0.20, 0.25) the addition of tin decreased the sensitivity, which may be due to the low density of active sites on the surface and lower probability of forming pairs of electrons and holes, thus reducing the interaction with gas molecules.

For gas sensing, response and recovery times are particularly critical. Figure 8 and Table 5 show the results of the response and recovery times of the nanoferrite $CdFe_2O_4$ -SnO_2 when exposed to hydrogen sulfide gas (H_2S), the effect of response and recovery times on operating temperature, and the addition of impurities. The sample (x = 0.15) had short response and recovery times (8.1- 42.3s) at 200°C-250°C. This can arise from the reality that the sample has a small grain size and high porosity, which means a more active surface toward hydrogen sulfide gas. This led to an increase in oxygen flow during the preparation of the sensor samples, which led to a reduction in oxygen absorption on the surface and the extraction of conductive electrons from the region near the surface, which led to the formation of a surface layer free of electrons [42].

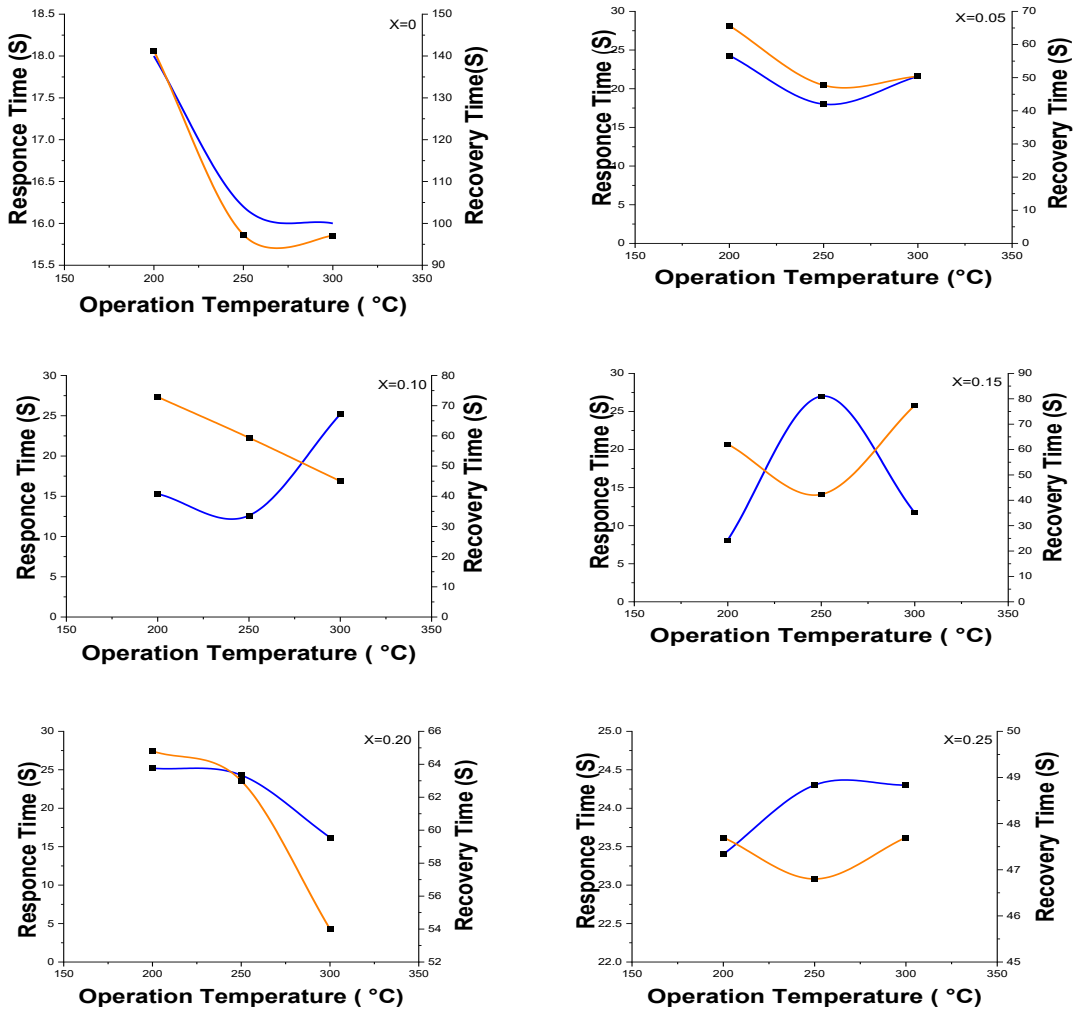

Figure 8: The relationship between H_2S gas response and recovery times at operating temperature for $CdFe_2O_4$ -SnO_2 samples: response time is shown by the blue line, while recovery times are shown by the red line.

Table 5: Minimum response and recovery time for $CdFe_2O_4$-SnO_2 samples to H_2S gas.

Content x	Minimum Response Time (S)	Operating Temperature (°C)	Minimum Recovery Time (S)	Operating Temperature (°C)
0	16.2	250°C	97.2	250°C
0.05	18	250°C	47.7	250°C
0.10	12.6	250°C	45	300°C
0.15	8.1	200°C	42.3	250°C
0.20	16.2	300°C	54	300°C
0.25	23.4	200°C	46.8	250°C

4. Conclusion

The nano ferrite $CdFe_2O_4$ -SnO_2 was prepared using a simple, spontaneous combustion (sol-gel) technique. X-ray diffraction analysis confirmed the formation of the single-phase cubic spinel structure. Confirmation was obtained for the formation of a single-phase cubic spinel structure. Using Scherrer and Williamson-Hall analysis, the grain size of the nanoscale was determined. Based on the scanning electron microscope image, the produced samples were mostly spherical. The structures mentioned in this work are appropriate for gas-sensing applications. The results of gas sensing measurements showed that the nanoferrite showed good sensitivity to H_2S at different operating temperatures. The sample (x=0.15) recorded the maximum sensitivity at 300°C with minimum response time at 200°C and minimum recovery time at 250°C, which means the nanoferrite $CdFe_2O_4$ -SnO_2 sensors are promising materials for sensing hydrogen sulfide H_2S.

References

[1] H. J. Kim, and J. H. Lee, "Highly sensitive and selective gas sensors using p-type oxide semiconductors: Overview," Sens. *Actuators B: Chem.,* vol. 192, pp. 607-627, 2014

[2] B. T. Raut, P. R. Godse, S. G. Pawar, M. A. Chougule, D. K. Bandgar, and V. B. Patil, "Novel method for fabrication of polyaniline–CdS sensor for H2S gas detection," Measurement., vol. 45, no. 1, pp. 94-100, 2012

[3] Y. Y. Xu, X. F. Rui, Y. Y. Fu, and H. Zhang, "Magnetic properties of α-Fe2O3 nanowires," *Chem. phys. lett*., vol. 410, no. 1-3, pp. 36-38, 2005.

[4] H. Yan, X. Su, C. Yang, J. Wang and C. Niu, "Improved photocatalytic and gas sensing properties of α-Fe2O3 nanoparticles derived from β-FeOOH nanospindles," *Ceram. Int*., vol. 40, no. 1, pp. 1729-1733, 2014.

[5] I.C. Nlebedim, N. Ranvah, P.I. Williams, Y. Melikhov, J.E. Snyder, A.J. Moses, and D.C. Jiles, "Effect of heat treatment on the magnetic and magnetoelastic properties of cobalt ferrite," *J. Magn. magn. mater.,* vol. 322, no. 14, pp. 1929-1933, 2010.

[6] D. S. Mathew and Ruey-Shin Juang, "An overview of the structure and magnetism of spinel ferritenanoparticles and their synthesis in microemulsions," *Chem. Eng. J.*, vol. 129, no. 1-3, pp. 51-65, 2007.

[7] N. Iftimie, E. Rezlesucu, P. D. Popa and N. Rezlescucu, "Gas sensitivity of nanocrystalline nickelferrite," *J. Optoelectron. Adv. Mater*., vol. 8, no. 3, pp. 1016-1018, 2006.

[8] A. V. Kadu, S. V. Jagtap, and G. N. Chaudhari. "Studies on the preparation and ethanol gas sensing properties of spinel Zn0. 6Mn0. 4Fe2O4 nanomaterials," *Curr. Apple. Phys.,* vol. 9, no. 6, pp. 1246-1251, 2009.

[9] H. Nathani, S. Gubbala, and R. D. K. Misra. "Magnetic behavior of nanocrystalline nickel ferrite: Part I. The effect of surface roughness," *Mater. Sci. Eng: B*., vol. 121, no. 1-2, pp. 126-136, 2005.

[10] Musab, Luma, and Entisar E. Al-Abodi. "Preparation and characterization composites contain of magnetic iron oxide nanoparticles with different weight ratios of dextrin, and using it to removal of heavy metals from aqueous solutions," *Energy Procedia.,* vol. 157, pp. 752-762, 2019.

[11] S. D. Shenoy, P. A. Joy, and M. R. Anantharaman, "Effect of mechanical milling on the structural, magnetic and dielectric properties of coprecipitated ultrafine zinc ferrite," *J. Magn. Magn. Mater.,* vol. 269, no. 2, pp. 217-226, 2004.

[12] W. Kim, S.W. Hyun, T. Kouh, C.S. Kim, and, E.J. Hahn, "Local magnetic properties of spinel Cd0.9M0.1Fe2O4 (M= Zn, Ni) investigated by using external magnetic field M¡ § ossbauer spectrometry," *Journal of the Korean Physical Society*, vol. 59, no. 6, pp. 3380-3384, 2011.

[13] K. S. Ramakrishna, C. Srinivas, C. L. Prajapat, S. S. Meena, M. V. K. Mehar, D. M. Potukuchi, and D. L. Sastry, "Structural and magnetic investigations: Study of magnetocrystalline anisotropy and magnetic behavior of 0.1% Cu^{2+} substituted Ni–Zn ferrite nanoparticles," *Ceram. Int*., vol. 44, no. 1, pp. 1193-1200, 2018.

[14] N.S., Chen, X.J., Yang, E.S. Liu, and J.L., Huang, "Reducing gas-sensing properties of ferrite compounds MFe2O4 (M= Cu, Zn, Cd and Mg)," *Sens. Actuators B: Chemi*., vol. 66, no. 1-3, pp. 178-180, 2000.

[15] N. Rezlescu, C. Doroftei, E. Rezlescu, and P. D. Popa. "The influence of Sn4+ and/or Mo6+ ions on the structure, electrical and gas sensing properties of Mg-ferrite," *phys. status solidi (a)* vol. 203, no. 2, pp. 306-316, 2006.

[16] A. Gurlo, N. Barsan, and U. Weimar. "Mechanism of NO2 sensing on SnO2 and In2O3 thick film sensors as revealed by simultaneous consumption and resistivity measurements," In *The 16th European Conference on Solid-State Transducers, Prague, Czech. Republic*, pp. 15-18. 2002.

[17] T. G. G. Maffeıs, G. T. Owen, M. W. Penny, T. K. H. Starke, S. A. Clark, H. Ferkel, and S. P. Wilks. "Nano-crystalline SnO2 gas sensor response to O2 and CH4 at elevated temperature investigated by XPS," Surf. *Sci*., vol. 520, no. 1-2, pp. 29-34, 2002.

[18] V. Manikandan, M. Singh, B.C. Yadav, R.S., Mane, S. Vigneselvan, A. Mirzaei and J. Chandrasekaran, "Room temperature LPG sensing properties of tin substituted copper ferrite (Sn− CuFe2O4) thin film," *Mater. Chem. Phys.,* vol. 240, p. 122265, 2020.

[19] Azhaar farouk Abd-Alzhra, "Synthesis and characterization and Study Electrical properties of Polymer composite containing Nanomaterials and use smart as materials," Thesis, University of Baghdad, College of Education for pure science/ Ibn-Al-Haitham, 2015.

[20] H. I. Mahdi, T. M. Al-Saadi, & N. A. Bakr, "Fabrication and characterization of $CoxMn_{0.25-x}Mg_{0.75}Fe_2O_4$ nanoparticles for H_2S sensing applications," Journal of Materials Science: Materials in Electronics, vol. 34, no. 22, p. 1634, 2023.

[21] K. Kumar, D. Vijaya, Paramesh, and P. Venkat Reddy. "Effect of aluminium doping on structural and magnetic properties of Ni-Zn ferrite nanoparticles." *World Journal of Nano Science and Engineering,* vol. 5, no. 03, p. 68, 2015.

[22] T. M. Al-Saadi, and M. A. Jihad, "Preparation of Graphene Flakes and studying its structural properties," *Iraqi J. Sc.,* vol. 57, no. 1A, pp.153-145, 2016.

[23] G. K., Salman, A. J. Bohan, and G. M. Jaed. "Use of nano-magnetic material for removal of heavy metals from wastewater," *Eng. Sci. Technol. J.,* vol. 35, no. 9A, pp. 903-908, 2017.

[24] A. R. A. Majeed, and A. E. Al-Robaie, "Study the Effect of Adding Citric Acid as a Fuel on the Structural Characteristics of the Nano Spinel Ferrite (Ni0. 1Cu0. 2Zn0. 7Fe2O4) Synthesized by Sol–Gel Auto Combustion Method," Ibn *Al-Haitham Journal for Pure and Applied Sciences*, vol. 28, no. 3, (2015).

[25] D. Ahmad, A. Ali, Z. Abbas, A. Zaman, A.M. Alsuhaibani, V. Tirth, M.R. Sarker, N.A.M Kamari, A. Algahtani, and M. Aljohani, "Structural, optical and dielectric properties of holmium-doped nickel-cadmium ferrite nanoparticles synthesized by sol-gel auto-combustion method," Crystals, vol.13, no. 3, p. 495, 2023.

[26] R. Ghasemi, J. Echeverría, J. I. Pérez-Landazábal, J. J. Beato-Lopez, M. Naseri, and C. Gómez-Polo, "Effect of Cu substitution on the magnetic and magnetic induction heating response of CdFe2O4 spinel ferrite," *J. Magn. Magn. Mater.,* vol. 499, p.166201, 2020.

[27] D.S. Nikam, S.V. Jadhav, V.M. Khot, R.A. Bohara, C.K. Hong, S.S. Mali, and S.H. Pawar, "Cation distribution, structural, morphological and magnetic properties of $Co_{1-x}Zn_xFe_2O_4$ (x=0-1) nanoparticles," *RSC Advances* vol.5, no. 3, pp.2338-2345, 2015.

[28] N. Rezlescu, C. Doroftei, E. Rezlescu, and P. D. Popa. "The influence of Sn4+ and/or Mo6+ ions on the structure, electrical and gas sensing properties of Mg-ferrite," *physica status solidi (a)* vol. 203, no. 2, pp. 306-316, 2006.

[29] R. Benrabaa, A. Löfberg, A. Rubbens, E. Bordes-Richard, R. N. Vannier, and A. Barama. "Structure, reactivity and catalytic properties of nanoparticles of nickel ferrite in the dry reforming of methane," *Catalysis today,* vol. 203, pp.188-195, 2013.

[30] Y. Köseoğlu, "Rapid Synthesis of Nanocrystalline NiFe2O4 and CoFe2O4 Powders by a Microwave-Assisted Combustion Method," *J. supercond. nov. magn.,* vol. 26, pp. 1391-1396, 2013.

[31] J. Xiang, Y. Chu, X. Shen, G. Zhou, and Y. Guo, "Electrospinning preparation, characterization and magnetic properties of cobalt–nickel ferrite (Co1− xNixFe2O4) nanofibers," *J. colloid interface sci.,* vol. 376, no. 1, pp.57-61, 2012.

[32] G. Korotcenkov, "Metal oxides for solid-state gas sensors: What determines our choice?" *Mater.Sci. Eng. B,* vol. 139, no. 1, pp. 1-23, 2007.

[33] A. Sutka, G. Mezinskis, A. Lusis, and M. Stingaciu. "Gas sensing properties of Zn-doped p-type nickel ferrite," *Sens. Actuators B: Chemi.,* vol.171, pp.354-360, 2012.

[34] R. Chen, W. Wang, X. Zhao, Y. Zhang, S. Wu, and F. Li, "Rapid hydrothermal synthesis of magnetic CoxNi1− xFe2O4 nanoparticles and their application on removal of Congo red," *Chem. Eng. J.,* vol. 242, pp. 226-233, 2014.

[35] Hussain, Farouq I., and Rusul Alaa Najem. "La+ 3 effectiveness replacement on the ferrite material (Cu0, 2Zn0, 45LaxFe2-xO4) On the structural and electrical and magnetic features," *Journal of Physics: Conference Series*. vol. 1003, no. 1, IOP Publishing, 2018.

[36] F. I. Hussain, "Synthesis of Nano Compound (Ba1-xSrxTiO3) by Sol-Gel Method and Study its Structural Properties," *Ibn Al-Haitham Journal for Pure and Applied Sciences*, vol.29, no. 1, pp. 417-427, 2016.

[37] A. A. R. Nemea, and B. I. Al-Abdaly, " Synthesis and Characterization Two Nanocomposites of Fe3O4 Nanoparticles and Using Them as a Chemical Sensors," *Ibn AL-Haitham Journal for Pure and Applied Sciences*, vol. 37, no. 3, pp. 216-228, 2024.

[38] M. A. Almessiere, B. Unal, Y. Slimani, H. Gungunes, M. S. Toprak, N. Tashkandi, A. Baykal, M. Sertkol, A.V. Trukhanov, A. Yıldızand, A. Manikandan, " Effects of Ce–Dy rare earths co-doping on various features of Ni–Co spinel ferrite microspheres prepared via hydrothermal approach," *Journal of Materials Research and Technology*, vol. 14, pp.2534-2553, 2021.

[39] A. Gurlo, M. Sahm, A. Oprea, N. Barsan, and U. Weimar, "A p-to n-transition on α-Fe2O3-based thick film sensors studied by conductance and work function change measurements," *Sensors and Actuators B: Chemical*, vol. 102, no. 2, pp. 291-298, 2004

[40] L. Saheb, and T. M. Al-Saadi, "Study of (Zn0. 7 Mn0. 3-x Ag0. 3 Fe2O4) ferrite nanoparticles synthesized by auto combustion method for NO_2 gas sensing," In AIP Conference Proceedings, vol. 2591, no. 1, AIP Publishing, 2023,

[41] T. Das, S. Mojumder, S. Chakraborty, D. Saha, and M. Pal, "Beneficial effect of Sn doping on bismuth ferrite nanoparticle-based sensor for enhanced and highly selective detection of trace formaldehyde,' *Applied Surface Science*, vol. 602, p.154340, 2022.

[42] W. K., Mahmood, T. M., Rashid, M. I., Rahmah, A. M., Jasim, M. Q., Fahem, M. S. Jabir, D.A., Abid, R.A., Majed, D.M. Awaid, & H. M., Yosif, "Empowering NO_2 detection: synthesis of highly responsive Au/Cu-doped iron oxide nanoparticles as gas sensors through laser ablation," Plasmonics, 1-10, 2024.